Electronic Supplementary Material (ESI) for Materials Advances.

Supporting Information for

Rapid Fabrication of MOF-based Mixed Matrix Membranes through Digital Light Processing

Alexey Pustovarenko, Beatriz Seoane, Edy Abou-Hamad, Helen E. King, Bert M. Weckhuysen, Freek Kapteijn and Jorge Gascon.*

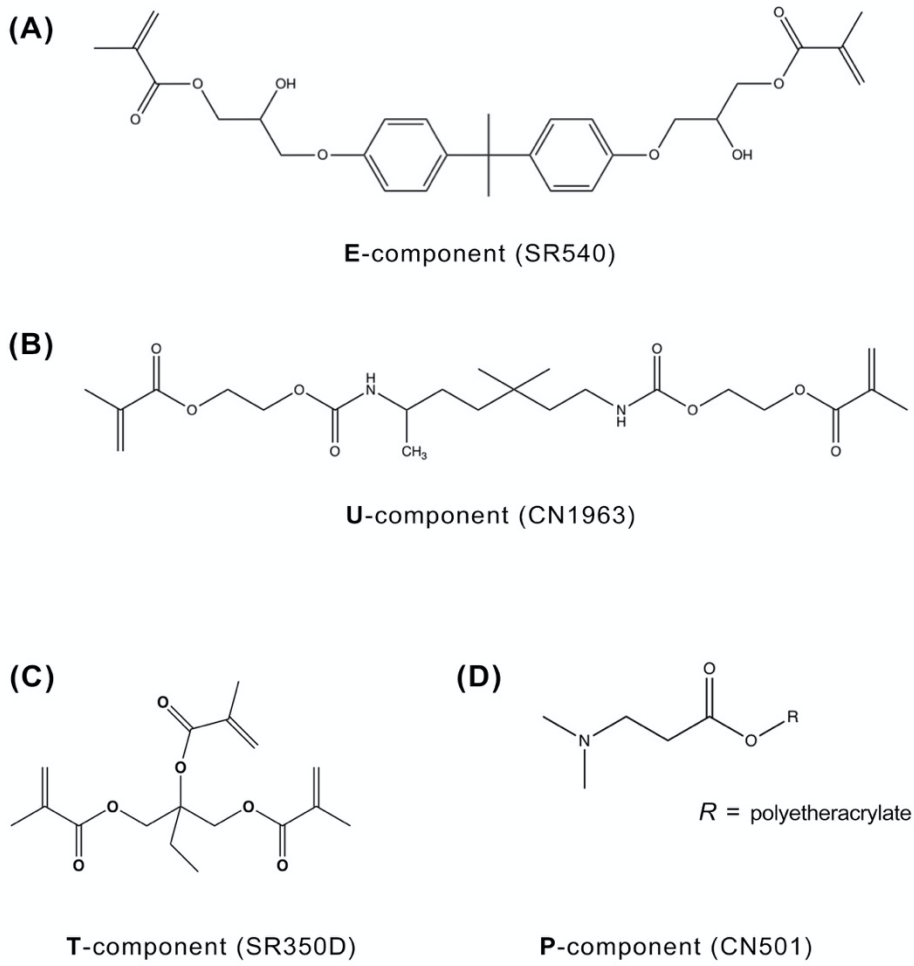

Figure S1. Chemical schemes and corresponding codes for photopolymerizable oligomers used in this study: (A) ethoxylated-4-bisphenol-A-dimethacrylate (**E**-component), (B) aliphatic urethane dimethacrylate (**U**-component), (C) trimethylolpropane trimethacrylate (**T**-component) and (D) amine modified polyether acrylate (**P**-component).

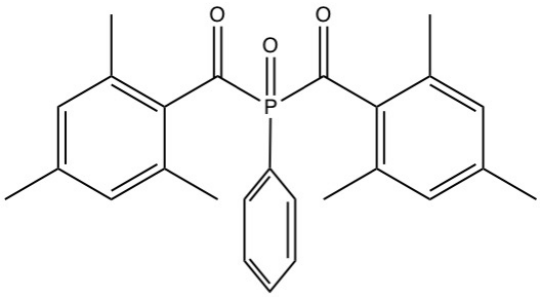

Figure S2. Chemical scheme of photoinitiator Irgacure®-819.

Table S1. Summary of photopolymerizable systems and MIL-53(Al)-NH_2/MMA containing ink formulations.

Entry	Sample code	Commercial oligomer [a]		Photoinitiator Irgacure®-819 [wt.%]	MIL-53-NH_2/MMA [wt.%]
		1st [wt.%]	2nd [wt.%]		
1	**T**-comp.	98	–	2	–
2	**P**-comp.	98	–	2	–
3	**U**-comp.	98	–	2	–
4	**E**-comp.	98	–	2	–
5	2/3**T**+1/3**U** -comps.	65	33	2	–
6	2/3**T**+1/3**E** -comps.	65	33	–	–
7	**T** / MIL-53-NH_2/MMA	86	–	2	12
8	**P** / MIL-53-NH_2/MMA	86	–	2	12
9	**U** / MIL-53-NH_2/MMA	86	–	2	12
10	**E** / MIL-53-NH_2/MMA	86	–	2	12
11	2/3**T**+1/3**E** / MIL-53-NH_2/MMA	58	28	2	12

[a] Acrylate systems contain 4-methoxyphenol as a stabilizer (~ 500-600 ppm)

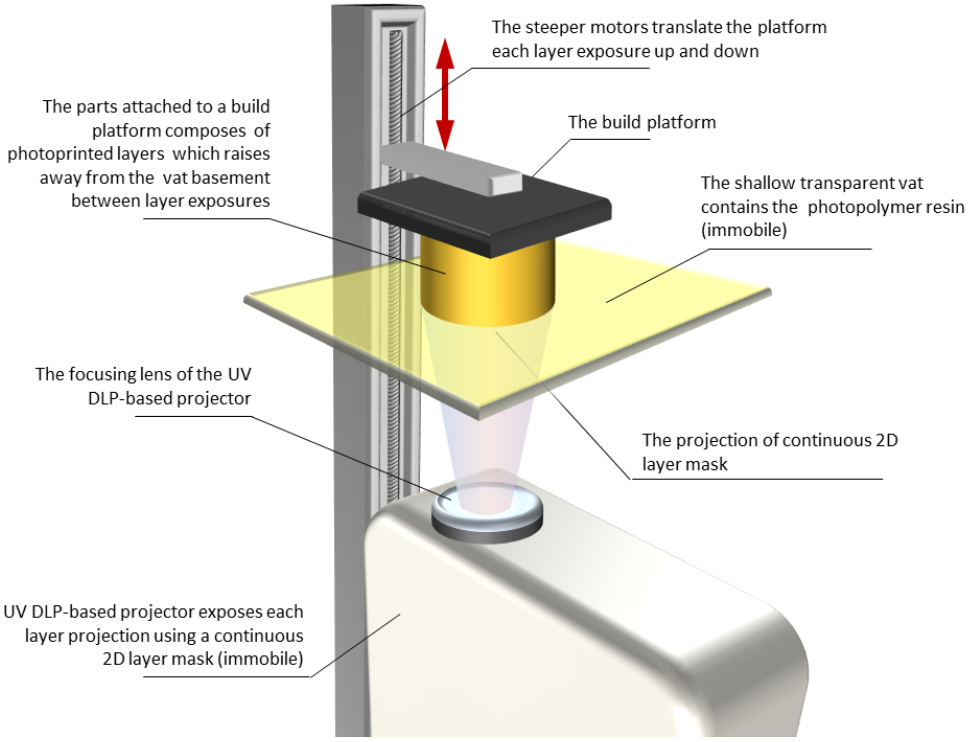

Figure S3. Scheme of 3D printer with DLP configuration.

The DLP printer setup consists of three main components: the projector, the resin basin (vat) and the build platform. The projector is placed under the transparent vat. The build platform enters the vat from the top and can be moved upwards to “pull” the print out of the vat layer by layer.

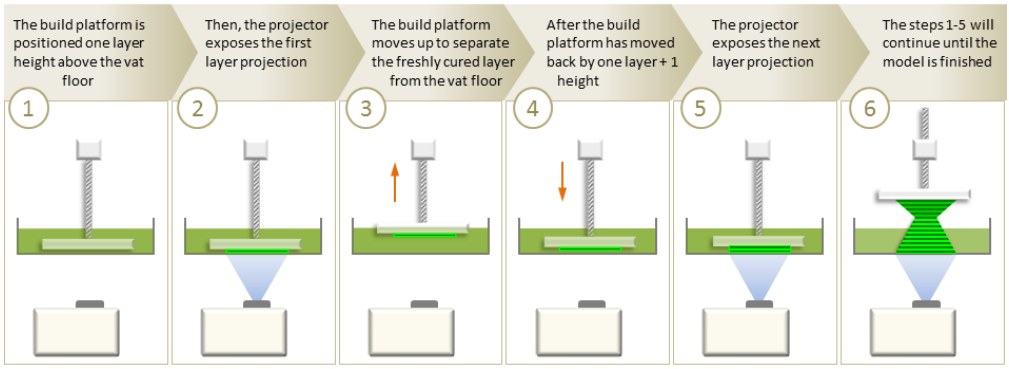

Figure S4. The six-step printing process using 3D DLP printer.

Table S2. Technical characteristics of 3D DLP printer Kudo3D model Titan 2.

Specifications		DLP Kudo3D Titan 2
Hardware	Machine size	40.9 cm × 34.8 cm × 85.3 cm
	Weight	13.6 kg
	Resin container	Flexible PSP
	Linear stage module	THK's high precision
	Projector	ACER H5360 LED DLP projector with a 2 cm native 1920 × 1080 DMD chip by Texas Instruments
Printing properties	XY resolution	38 – 92 µm
	Finest *Z* resolution	5 µm
	Maximum build size	**XY: 92 µm resolution** 17.5 cm × 9.6 cm × 24.9 cm **XY: 100 µm resolution** 19.0 cm × 10.9 cm × 24.9 cm
	Maximum print speed (for XY = 50 µm and Z = 100 µm)	6.86 cm/h
Control	Control software	Web-based
	Connectivity	LAN cable
	Printer control	PC
Calibration and assembly	Pre-calibration	At 50 µm / 75 µm
	Assembly	Fully assembled body

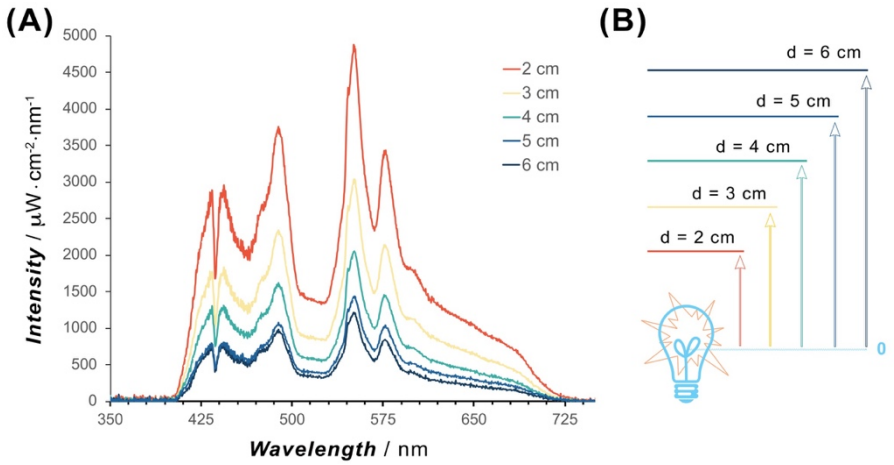

Figure S5. (A) Spectral irradiance of the 3D printer light source as a function of the distance (B) between the printer light source and resin vat.

Table S3. Typical operative parameters for DLP 3D printing used in this study.

Parameter	Value
Exposure time	10 [s]
Layer thickness	50 [μm]
Lifting height	3.5 [mm]
Lifting speed	10 [mm·min^{-1}]
Projected width	28 [mm]
Projected length	49.8 [mm]
Projected area	1393.7 [mm^2]
Temperature	RT
Light intensity	212.5 [mW·cm^{-2}]

Table S4. Summary of power density of the 3D printer light source as a function of the separation distance between the printer light source and resin vat.

d [cm]	P [mW·cm^{-2}]
2	566.6
3	240.3
4	212.5
5	164.3
6	137.3

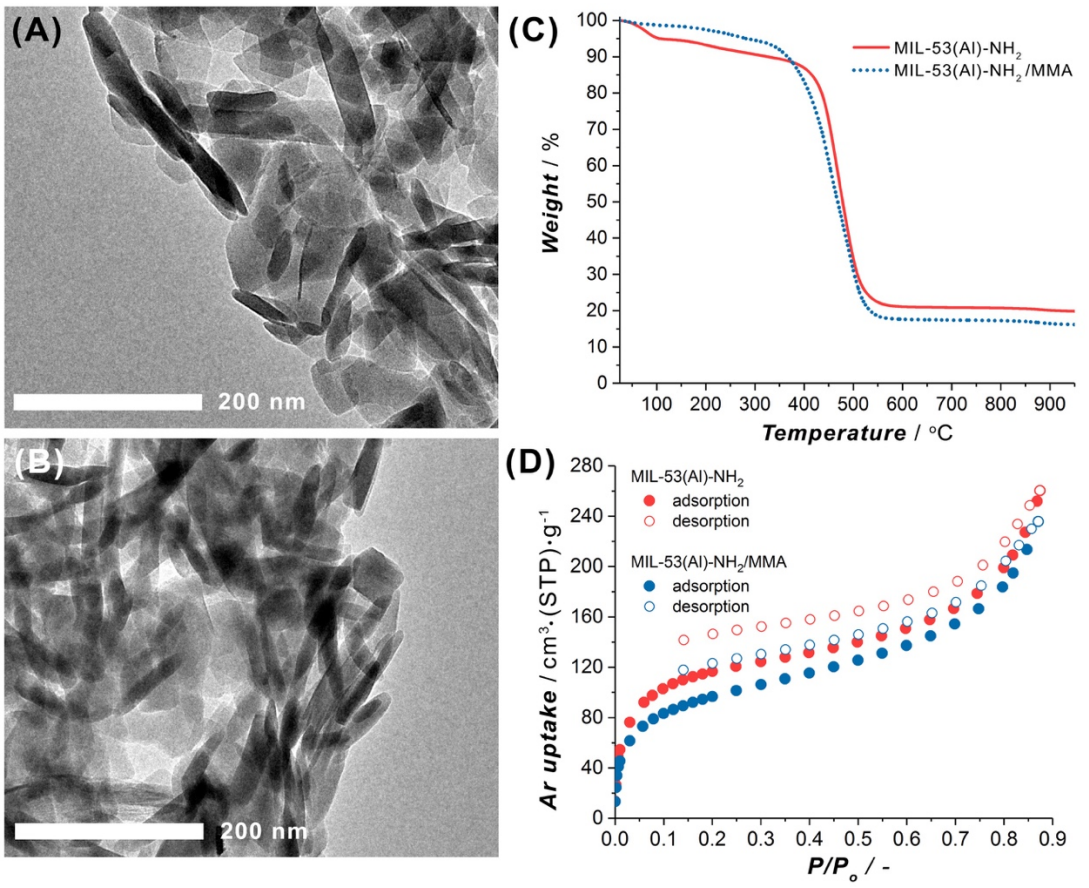

Figure S6. TEM images of MIL-53(Al)-NH_2 (A) and MIL-53(Al)-NH_2/MMA (B). Thermogravimetric curves in air atmosphere (C) and N_2 adsorption isotherms (D) for MIL-53(Al)-NH_2 and MIL-53(Al)-NH_2/MMA.

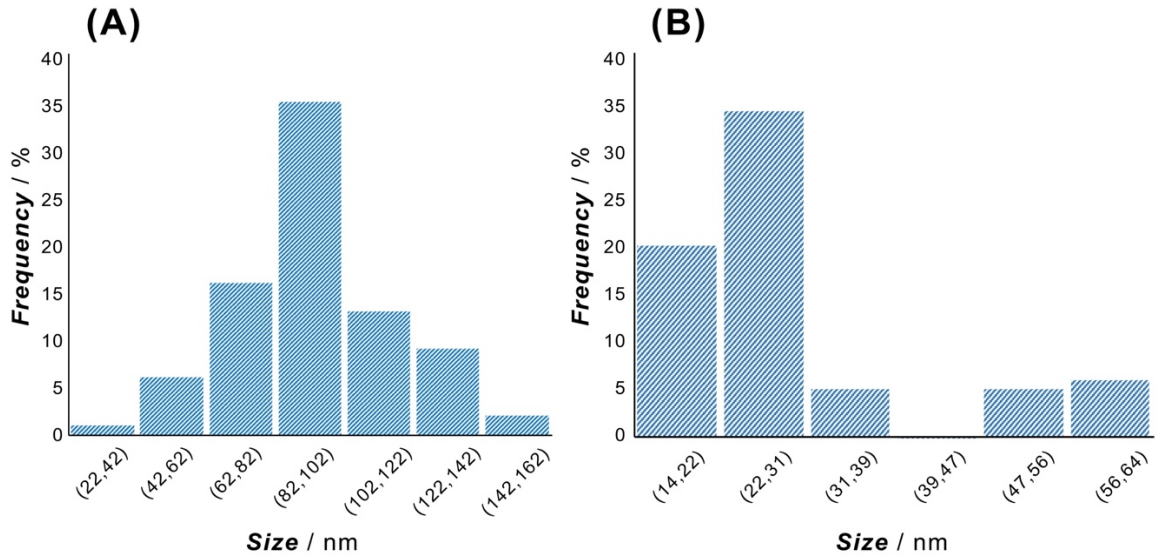

Figure S7. Particle size distributions of MIL-53(Al)-NH_2 nanoparticles measuring (A) length (mean of 95 ± 24 nm) or (B) width (mean of 28 ± 13 nm). Measurements were performed on several TEM images accounting of more than 100 particles.

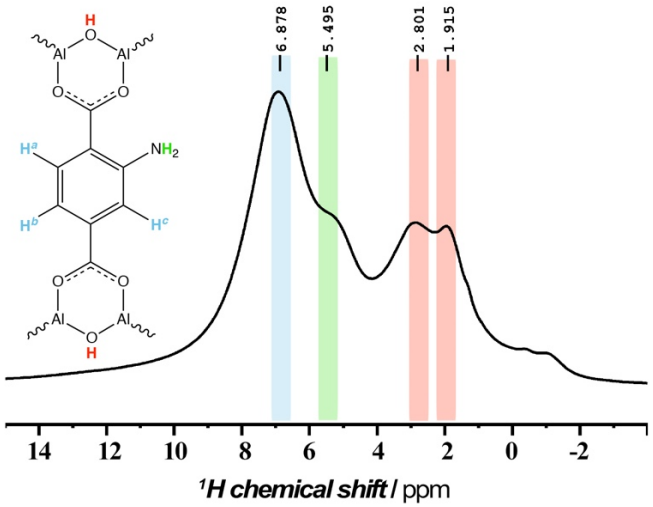

Figure S8. Solid-state one-dimensional ^1H MAS NMR spectrum of MIL-53(Al)-NH_2 before post-synthetic modification.

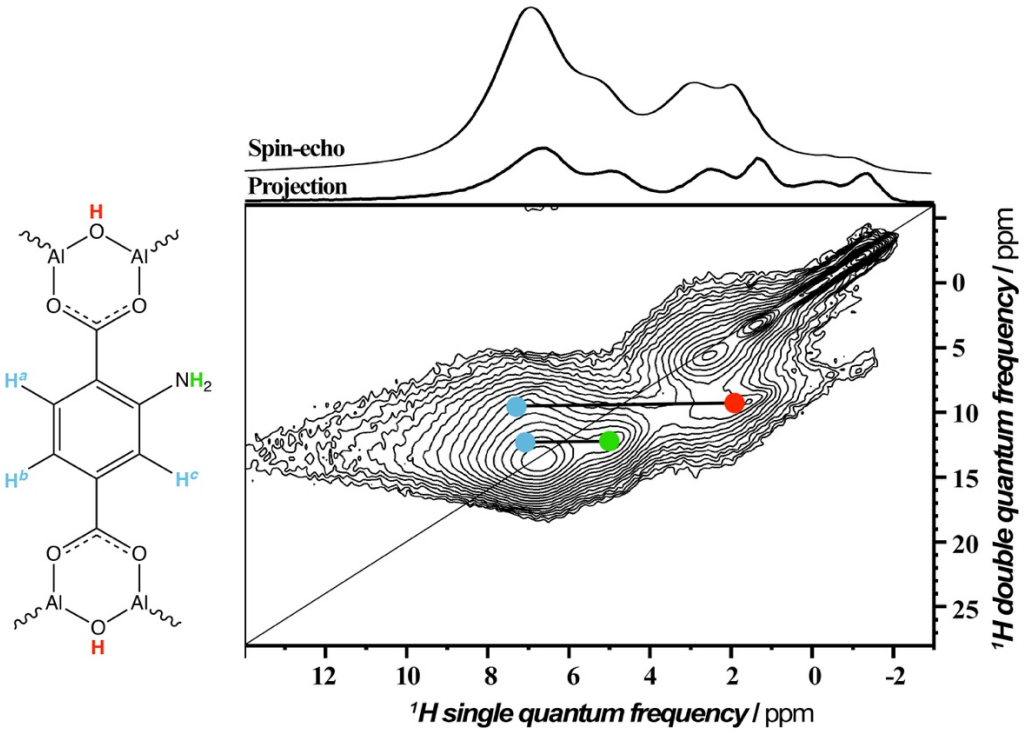

Figure S9. Solid state 2D ^{1}H MAS DQ-SQ NMR correlation spectrum for MIL-53(Al)-NH_2 before post-synthetic modification.

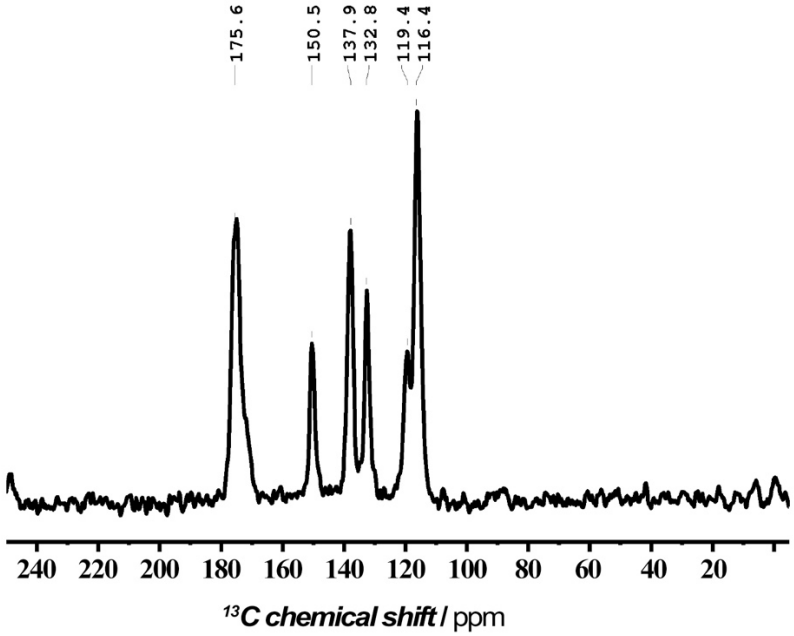

Figure S10. Solid-state one-dimensional ^{13}C CP-MAS NMR spectrum of MIL-53(Al)-NH_2 before post-synthetic modification.

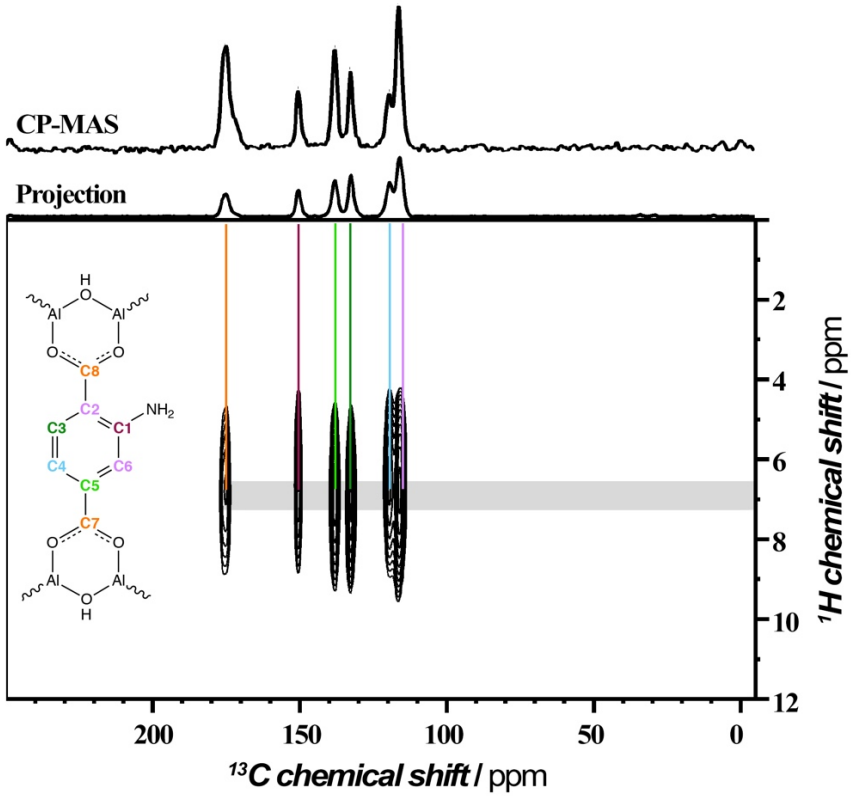

Figure S11. Solid-state two-dimensional (2D) ^{13}C-^{1}H heteronuclear single quantum correlation NMR spectrum of MIL-53(Al)-NH_2 before post-synthetic modification.

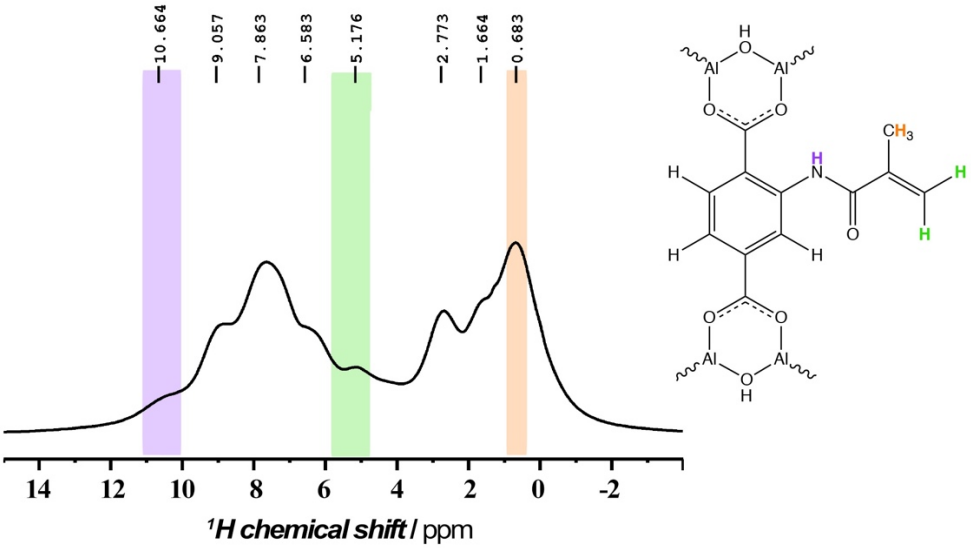

Figure S12. Solid-state ^{1}H MAS NMR spectrum of MIL-53(Al)-NH_2/MMA after post-synthetic modification. Characteristic resonances expected to be in PSM material with MMA moiety are shown in color.

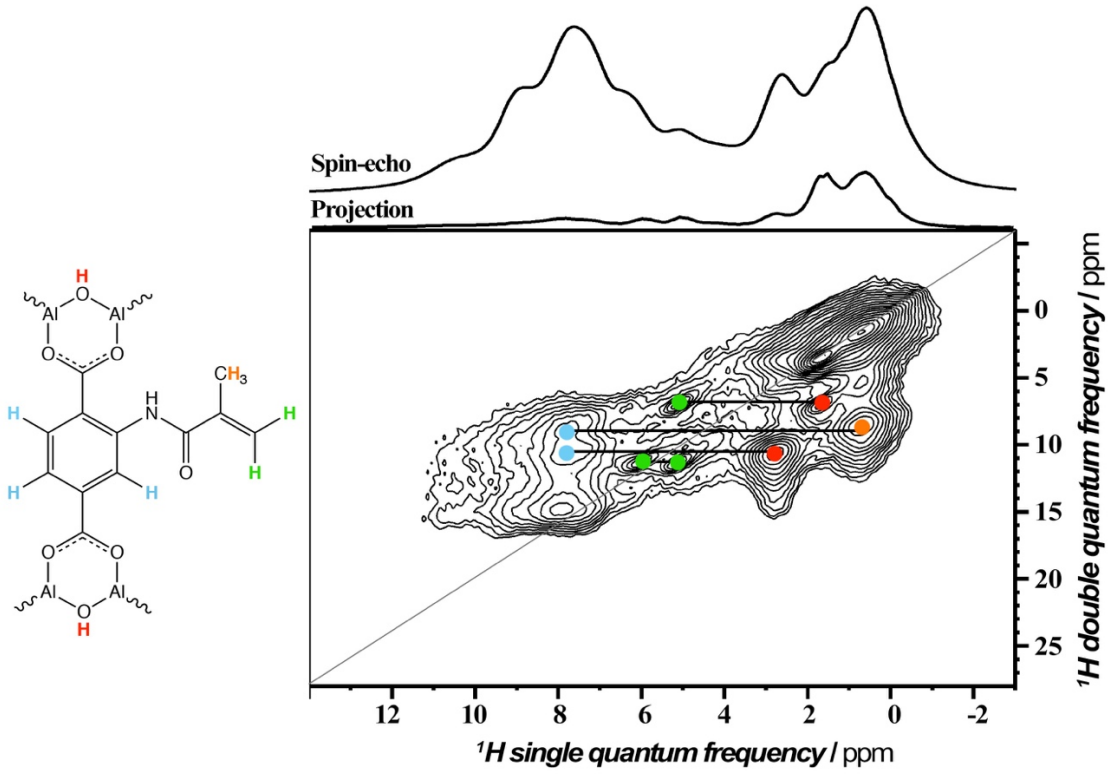

Figure S13. Solid-state 2D ^{1}H MAS DQ-SQ NMR correlation spectrum of MIL-53(Al)-NH_2/MMA after post-synthetic modification.

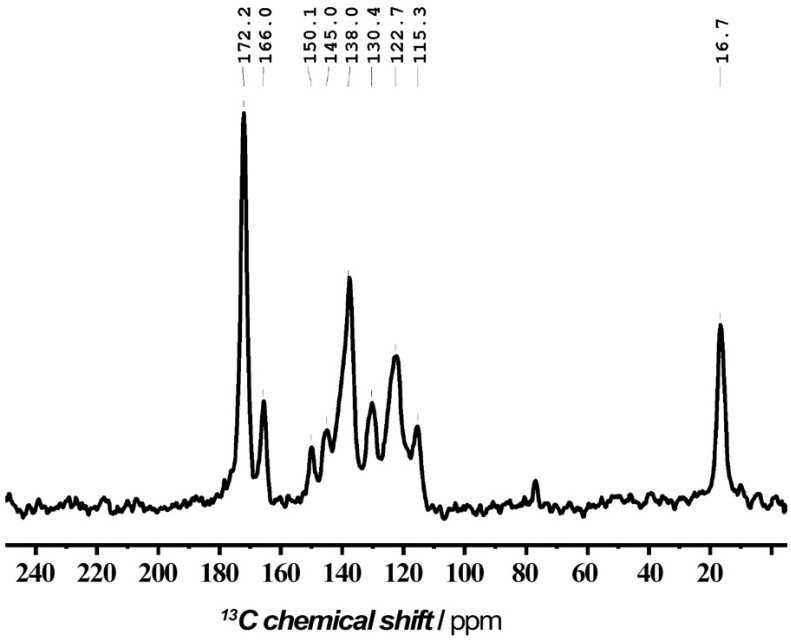

Figure S14. Solid-state ^{13}C CP-MAS NMR spectrum of MIL-53(Al)-NH_2/MMA after post-synthetic modification.

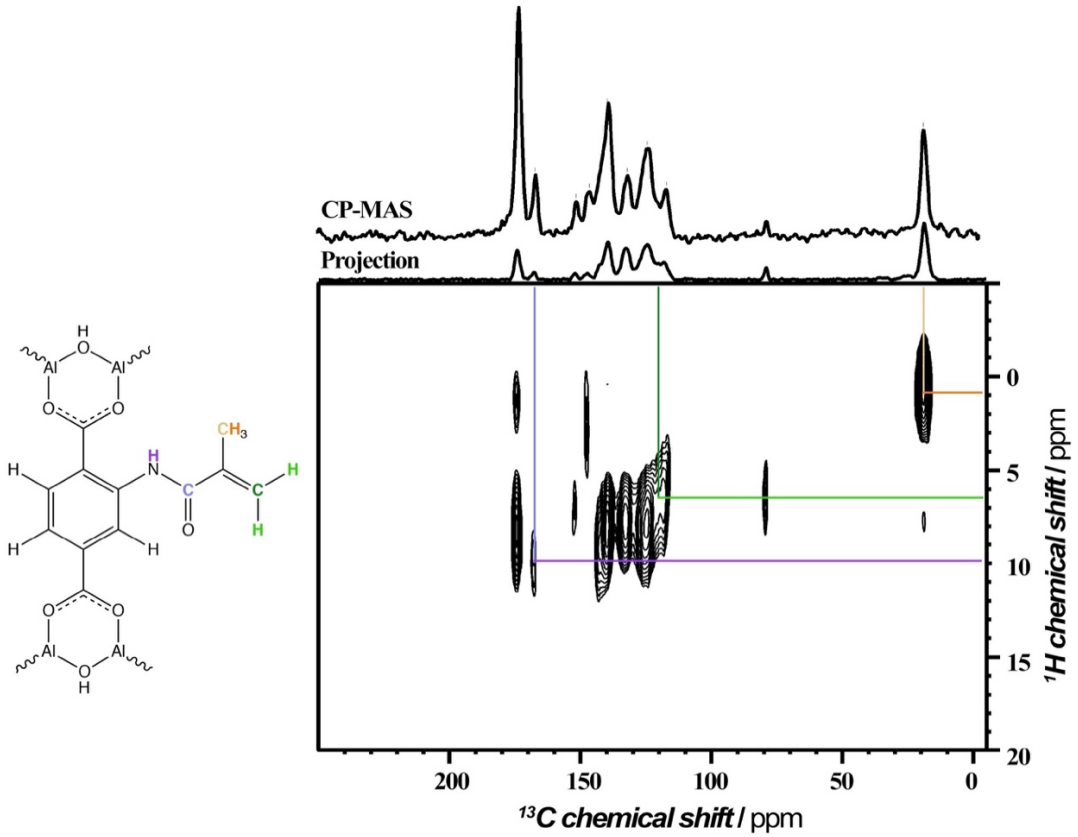

Figure S15. Solid-state two-dimensional (2D) ^{13}C-^{1}H heteronuclear single quantum spectrum of MIL-53(Al)-NH_2/MMA after post-synthetic modification.

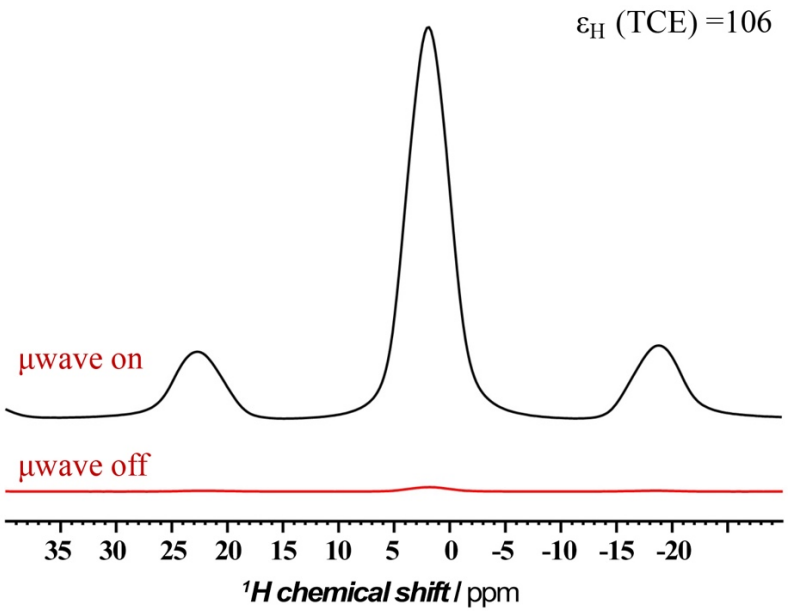

Figure S16. Solid-state DNP enhanced ^{1}H NMR spectrum of MIL-53(Al)-NH_2 before post-synthetic modification with and without DNP microwave applied.

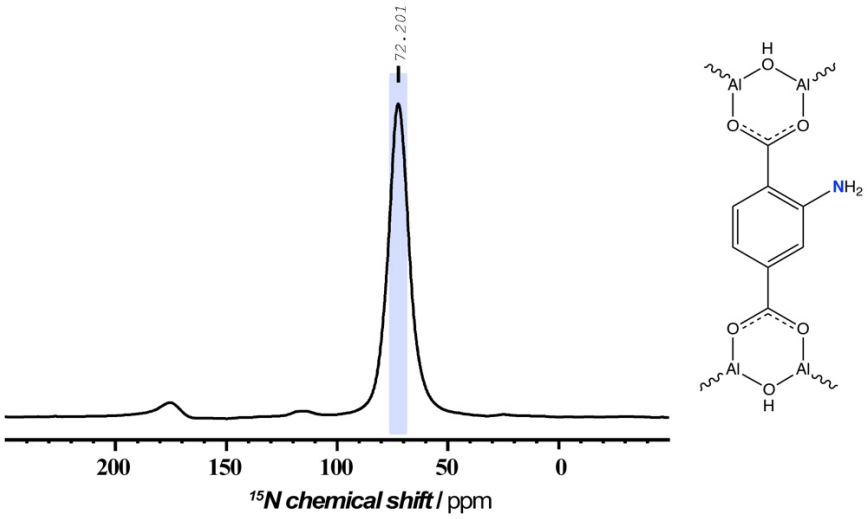

Figure S17. Solid-state DNP enhanced ^{15}N NMR spectrum of MIL-53(Al)-NH_2 before post-synthetic modification.

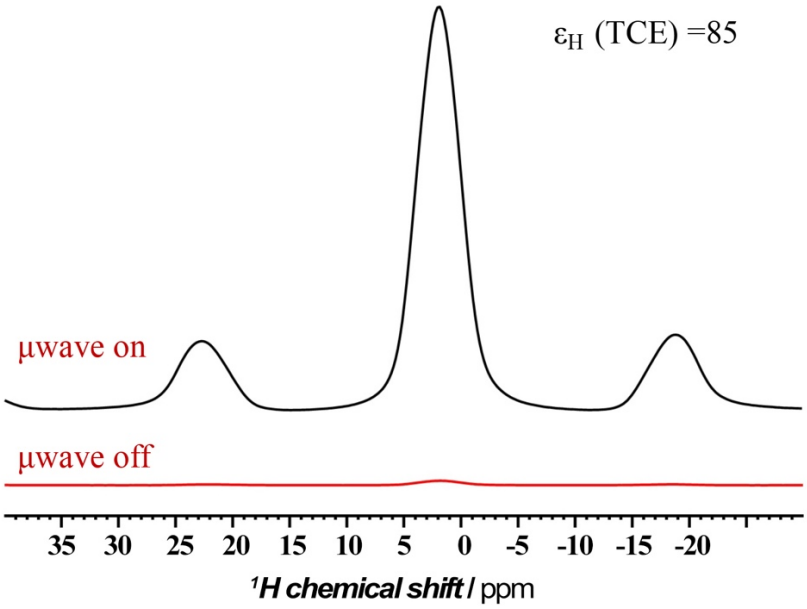

Figure S18. Solid-state DNP enhanced ^{1}H NMR spectrum of MIL-53(Al)-NH_2/MMA after post-synthetic modification with and without DNP microwave applied.

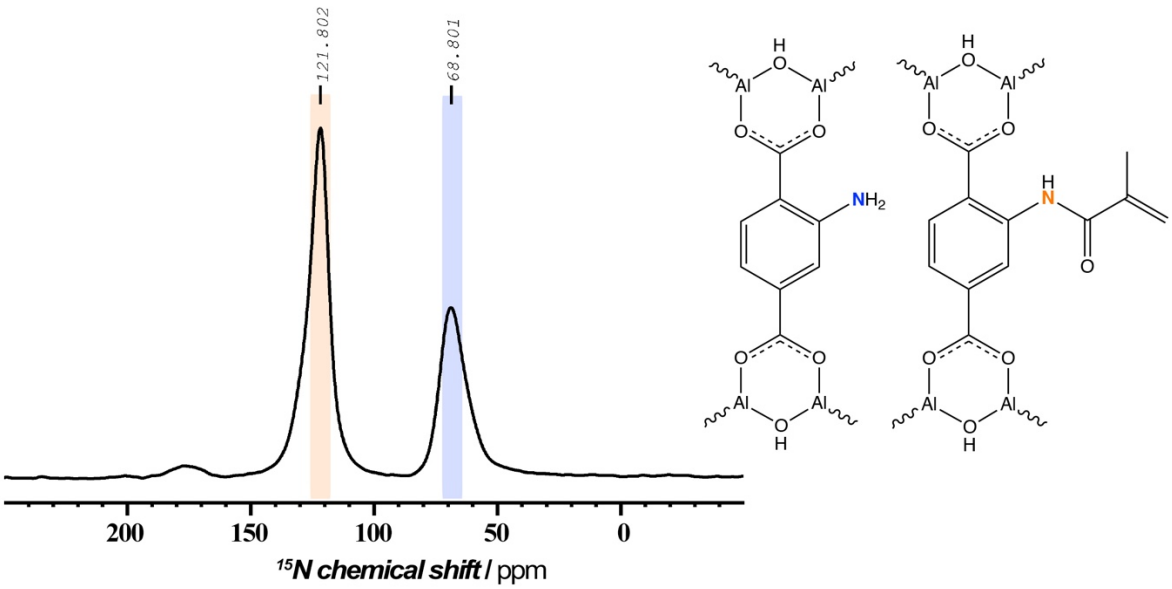

Figure S19. Solid-state DNP enhanced ^{15}N NMR spectrum of MIL-53(Al)-NH_2/MMA after post-synthetic modification.

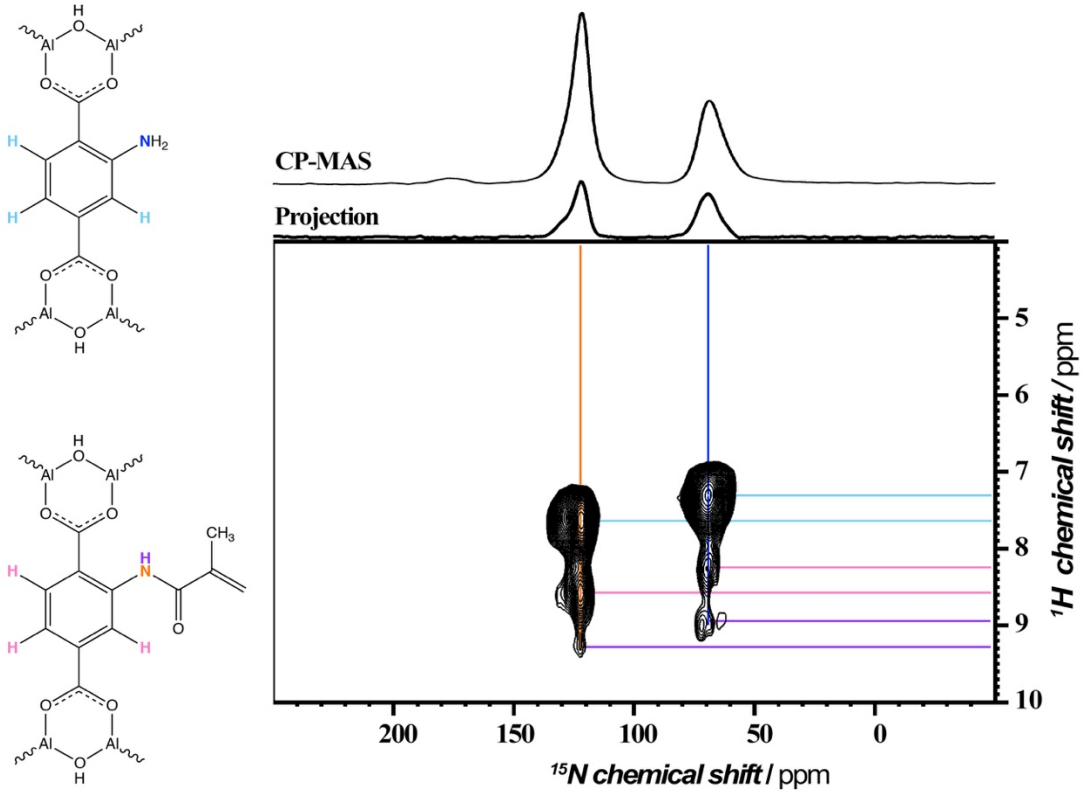

Figure S20. Solid-state DNP enhanced ^{15}N-^{1}H CP-MAS HETCOR NMR spectrum of MIL-53(Al)-NH_2/MMA after post-synthetic modification.

Table S5. TGA and Ar physisorption data for MIL-53(Al)-NH_2 and MIL-53(Al)-NH_2/MMA.

Sample	Surface area [$m^2 \cdot g^{-1}$]			TGA
	S_{BET}	S_{micro}	S_{ext} [a)]	$\Delta m/m_0$ [%] [b)]
MIL-53(Al)-NH_2	370	150	220	68
MIL-53(Al)-NH_2/MMA	303	43	260	80

[a)] Mesopore surface area is obtained from the *t*-plot applied to the Ar isotherm; [b)] Value corresponds to the mass loss step observed on thermogravimetric curve in region 350-600 °C

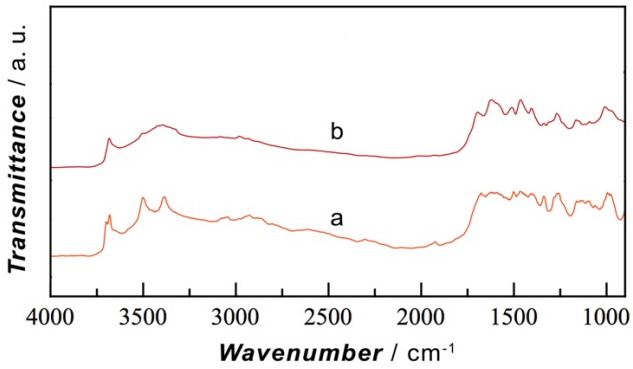

Figure S21. FTIR spectra of MIL-53(Al)-NH_2 before (a) and after (b) post-synthetic modification with MMA group.

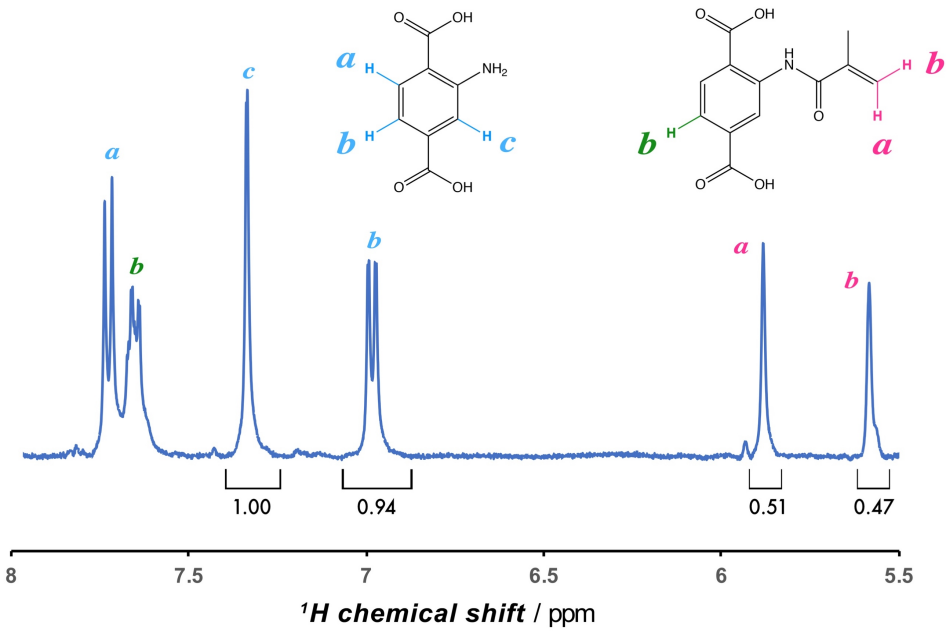

Figure S22. Liquid state ^{1}H NMR spectrum of MIL-53(Al)-NH_2/MMA digestion crude in DMSO-d6.

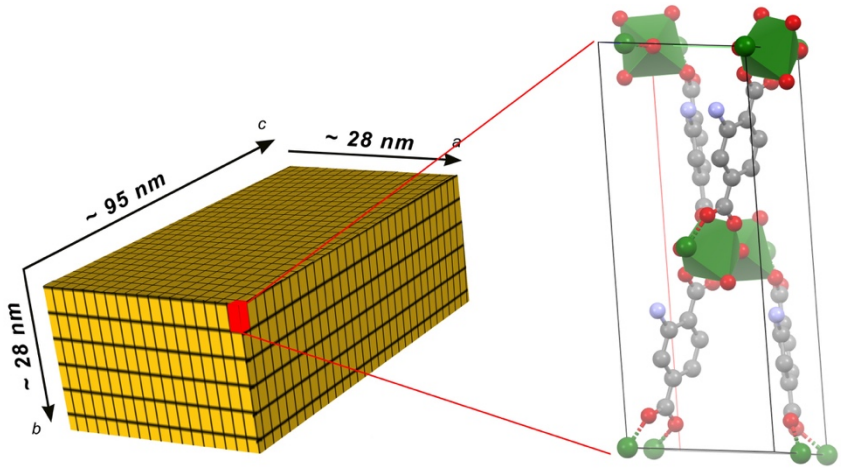

Figure S23. Schematic representation of MIL-53(Al)-NH_2 nanoparticle with ~95 nm × 28 nm × 28 nm dimensions (Figure S7) and unit cell arrangement of *np*-form of the framework with respect to the crystal faces. Image showing the surface fraction of the linkers (20%) exposed to PSM and structure orientation within unit cell respective to the nanocrystal facets.

Table S6. Viscosity of commercial photopolymerizable methacrylic systems at 25 °C.

Component	Sample code	Viscosity [cP]
SR350D	T	65.7
CN501	P	65
SR540	E	575
CN1963	U	1740

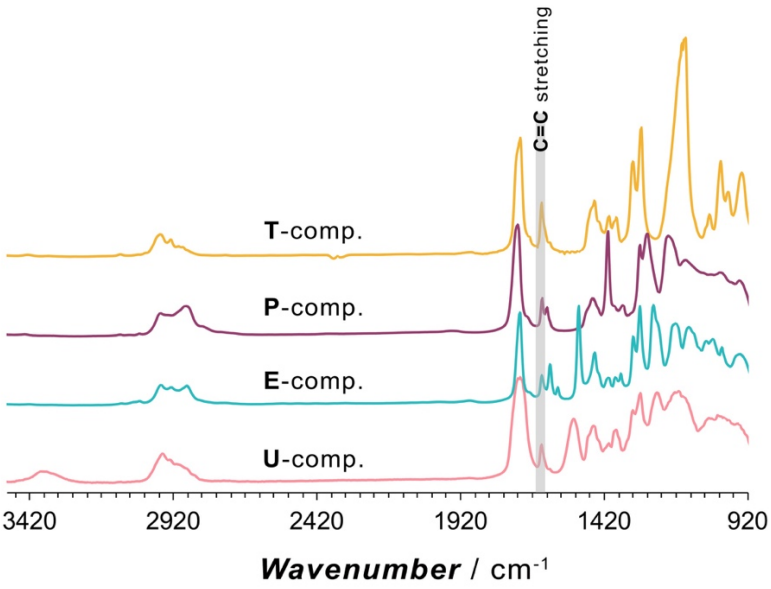

Figure S24. ATR-FTIR spectra for **T**-, **P**-, **E**- and **U**-components with the highlight of characteristic C=C stretching (~1640 cm^{-1}) of methacrylic group.

Table B7. Data of kinetic characteristics of photopolymerizable systems with and without MOF additive.

Components		Sample code	X_{MMA}^{total} [%]	$v_{XMMA}^{50\%}$ [%·s^{-1}]
Comm.	MOF			
SR350D	–	T	27	1.50
CN501	–	P	25	2.40
SR540	–	E	24	1.55
CN1963	–	U	15	0.75
SR350D	MIL-53-NH$_2$/MMA	**T**/MIL-53-NH$_2$/MMA	30	0.55
CN501	MIL-53-NH$_2$/MMA	**P**/MIL-53-NH$_2$/MMA	27	0.50
SR540	MIL-53-NH$_2$/MMA	**E**/MIL-53-NH$_2$/MMA	25	0.39

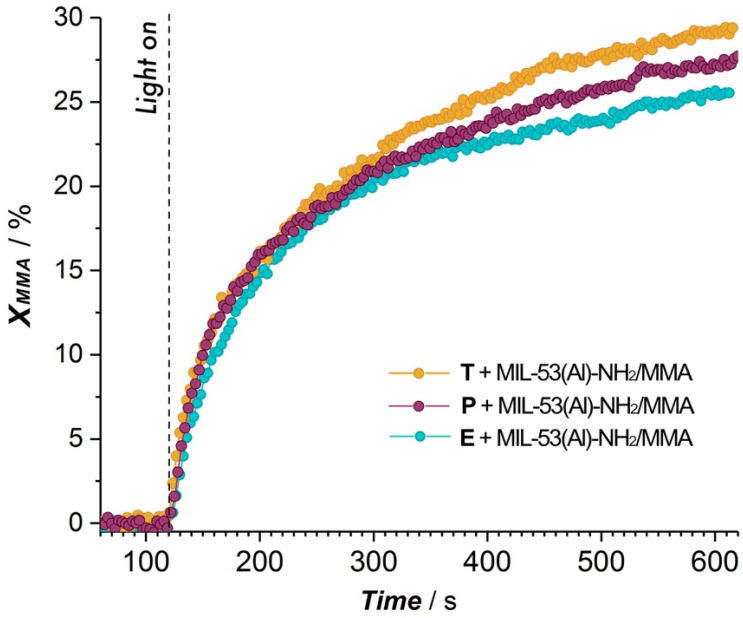

Figure S25. Methacrylate group conversion (X_{MMA}, %) curves for formulations containing MIL-53(Al)-NH$_2$/MMA and different oligomers.

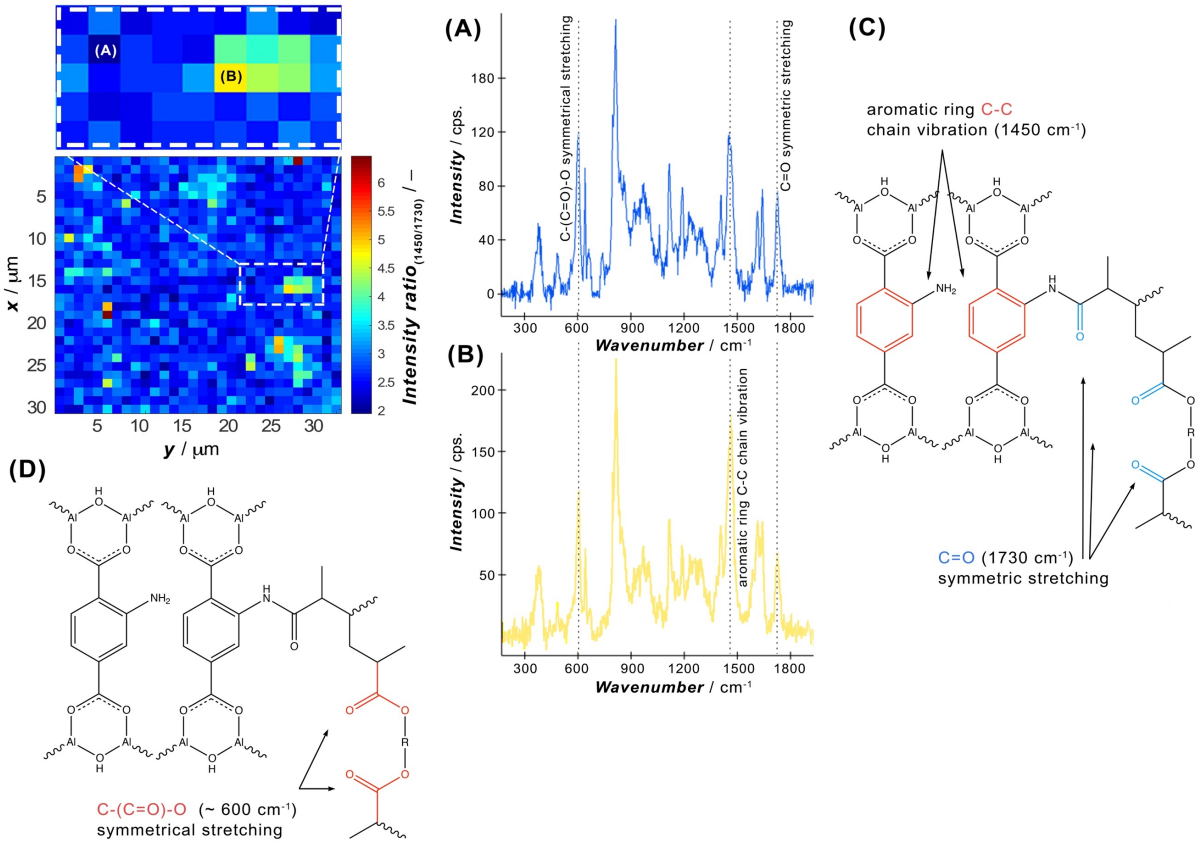

Figure S26. Raman map with the selected (A) and (B) pixels on the color scaled confocal microscopy map (inset) and Raman spectra (A) and (B) corresponding to these pixels. Dashed lines indicate the analyzed intensities: for the map shown in Figure 4A, the intensity corresponding to C-(C=O)-O (~ 600 cm^{-1}) symmetric stretching (D) in the MMA moieties involved in copolymerization was considered, whereas the map depicted on Figure 4B (and top left in above figure) was build based on relative intensities of the aromatic ring C-C chain vibration (1450 cm^{-1}) of the MOF's linker and C=O symmetric stretching (1730 cm^{-1}) (C) of the copolymerized moieties in the composite.

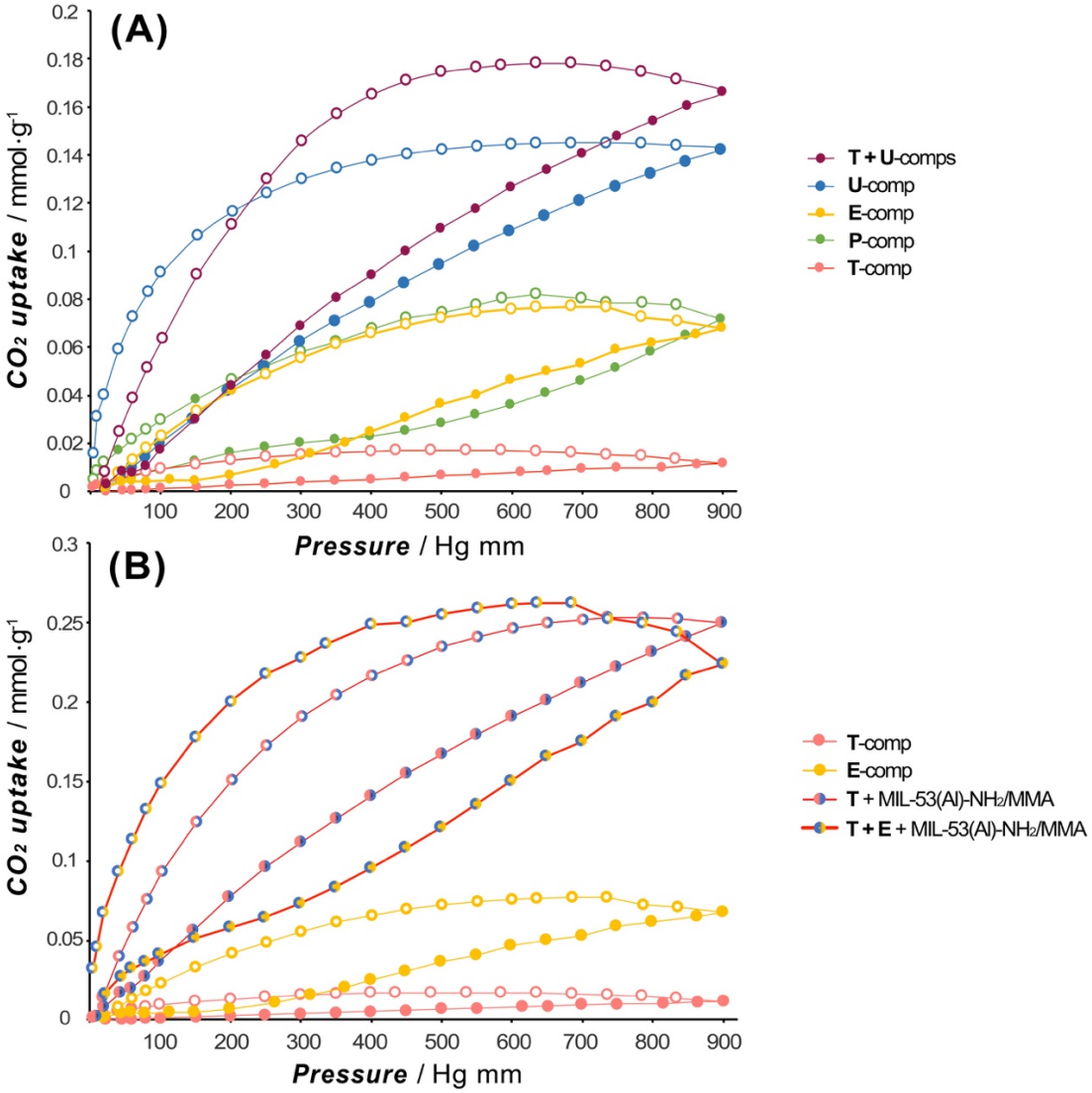

Figure S27. CO_2 adsorption isotherms of (A) membranes 3D printed from **T**-, **P**-, **E**- and **U**-commercial oligomers and **T**+**U** mixture, and (B) of membranes 3D printed from MIL-53(Al)-NH_2/MMA containing ink mixtures acquired at 273 K. Filled symbols correspond to the adsorption branch and open symbols to the desorption.

Table S8. Mechanical data of photopolymerizable systems and MIL-53(Al)-NH_2/MMA contained ink formulations.

Sample code	ε_R [%] [a]	σ_R [MPa] [b]	Young's modulus [GPa]	tan δ [–] [c]	δ [°] [d]
U-comp	0.67	50.6	7.6	0.092	5.25
T-comp	1.82	47.8	2.7	0.081	4.66
T / MIL-53-NH_2/MMA	1.20	26.0	2.2	0.076	4.36
P-comp	2.15	68.3	3.3	0.112	6.42
P / MIL-53-NH_2/MMA	1.25	44.4	3.6	0.091	5.20
E-comp	2.75	30.2	1.1	0.120	6.86
E / MIL-53-NH_2/MMA	0.80	11.9	1.6	0.113	6.47
2/3**T**+1/3**E**-comps	1.58	31.3	2.0	0.080	4.59
2/3**T**+1/3**E** / MIL-53-NH_2/MMA	1.04	25.9	2.5	0.071	4.06

[a] Strain at break (ε_R, %); [b] Stress at break (σ_R, MPa); [c] Phase difference in stress and strain (δ, degrees); [d] Damping factor (tan δ).

Mechanical analyses were performed on stress-strain data curves determining the strain at break (ε_R) and stress at break (σ_R) values by extrapolating the last point of the curve on abscise and ordinate axes, respectively.

Young's modulus was determined from corresponding stress-strain curves as a slope coefficient on the linear fits.

The damping properties of the composites during tension or compression were expressed in terms of the stress and strain relations, and defined by following Equation S1:

$$\tan\delta = \frac{E''}{E'} \qquad (S1)$$

where tan δ is so-called damping factor, E'' and E' are loss modulus and storage modulus, respectively.

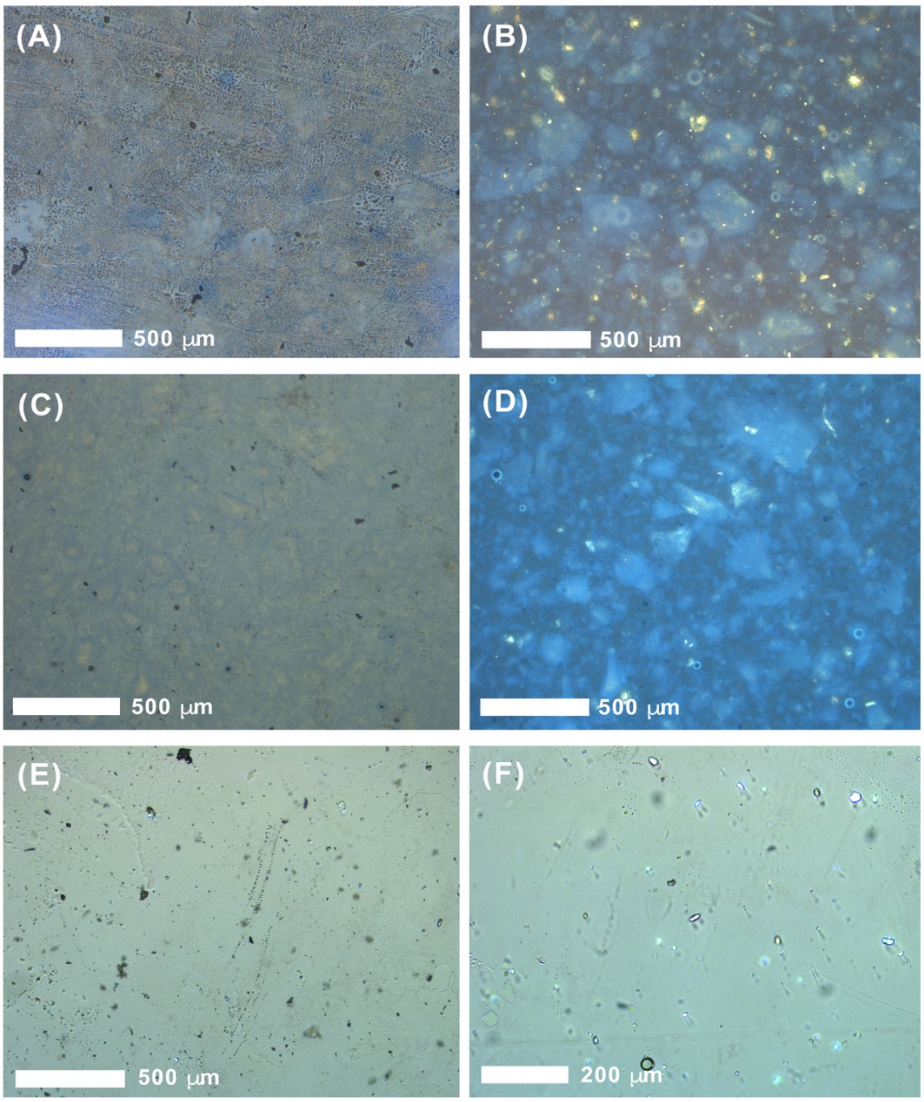

Figure S28. Micrographs of 3D printed composites containing MIL-53(Al)-NH_2/MMA in **T**-(A), **P**- (C) and **E**-matrix (E) under reflected light and (B, D, F) the same under crossed polarizers.

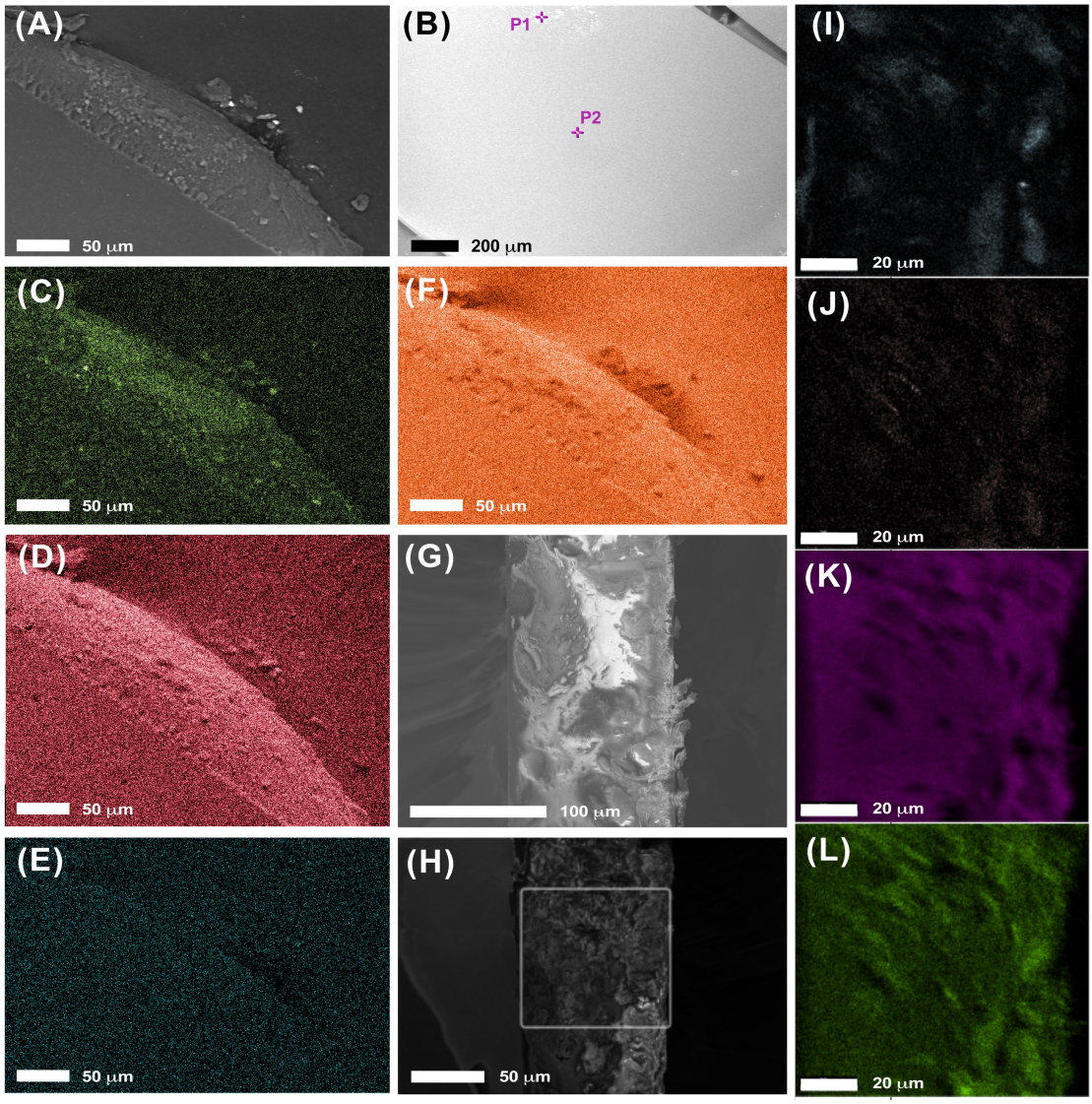

Figure S29. SEM-EDX maps of **T**/MIL-53(Al)-NH_2/MMA 3DP composite: (A) top view survey image and corresponding to Al (C), O (D), P (E), C (F) *K*-edges maps. (B) SEM image of the membrane and two locations used for the elemental analysis. (G) Cross-section view of the membrane and (H) survey image with the analyzed region for Al (I), N (J), C (K) and O (L) mappings.

Table S9. Elemental analysis data derived obtained by EDX from the two locations of 3DP membrane according to Figure S29B.

Element	Relative mass [%]	
	Point 1 (P1)	Point 2 (P2)
Al	1.42	1.81
C	76.81	69.54
O	21.47	28.49
P	0.30	0.16

Table S10. Degree of the crosslinking (DC, %) of photopolymerizable systems with and without MOF additive.

Components		Sample code	DC [%]
Comm.	MOF		
SR350D	–	**T**	96.2
CN501	–	**P**	97.4
SR540	–	**E**	99.7
CN1963	–	**U**	93.6
SR350D	MIL-53-NH_2/MMA	**T**/MIL-53-NH_2/MMA	93.9
CN501	MIL-53-NH_2/MMA	**P**/MIL-53-NH_2/MMA	94.7
SR540	MIL-53-NH_2/MMA	**E**/MIL-53-NH_2/MMA	92.8

Table S11. Thermogravimetric (TGA) and differential scanning calorimetry (DSC) data for photopolymerizable inks with and without MOF additive.

Components		Sample code	T_d [°C]	T_g [°C]	$\Delta m/m_0$ [%]
Comm.	MOF				
SR350D	–	**T**	461.0	155.7	96.5
CN501	–	**P**	432.5	84.4	98.0
SR540	–	**E**	428.0	180.4	97.3
CN1963	–	**U**	387.5	173.6	99.4
SR350D	MIL-53-NH_2/MMA	**T**/MIL-53-NH_2/MMA	438.0	145.3	87.3
CN501	MIL-53-NH_2/MMA	**P**/MIL-53-NH_2/MMA	429.5	79.5	89.7
SR540	MIL-53-NH_2/MMA	**E**/MIL-53-NH_2/MMA	432.5	190.3	86.3

T_d - temperature at which a maximum mass loss velocity is observed; T_g – glass transition temperature; Δm – total mass loss in air atmosphere.

Table S12. Summary of gas separation performance obtained with 3DP polymer and 3DP MOF-polymer composite membranes (12 wt.% MOF loading) under several operation conditions.

Membrane	**T**-comp.		**T** + MIL-53-NH_2/MMA	
Thickness (μm)	48 ± 2		57 ± 1	
Temperature	323 K	373 K	323 K	373 K
ΔP (bar)	1	1	1	1
P_{H2} (Barrer)	9.4 ± 0.4	42 ± 13	229 ± 79	501 ± 82
P_{CO2} (Barrer)	4.8 ± 1.4	40 ± 9	120 ± 14	346 ± 87
H_2/CO_2 selectivity (-)	1.9 ± 0.5	1.1 ± 0.1	1.9 ± 0.6	1.5 ± 0.2